

# Kinetic model for calcium sulfate $\alpha$ -hemihydrate produced hydrothermally from gypsum formed by flue gas desulfurization

Mingliang Tang, Xuerun Li, Yusheng Shen and Xiaodong Shen

*J. Appl. Cryst.* (2015). **48**, 827–835



**IUCr Journals**  
CRYSTALLOGRAPHY JOURNALS ONLINE

Copyright © International Union of Crystallography

Author(s) of this paper may load this reprint on their own web site or institutional repository provided that this cover page is retained. Republication of this article or its storage in electronic databases other than as specified above is not permitted without prior permission in writing from the IUCr.

For further information see <http://journals.iucr.org/services/authorrights.html>



# Kinetic model for calcium sulfate $\alpha$ -hemihydrate produced hydrothermally from gypsum formed by flue gas desulfurization

Mingliang Tang,<sup>a,b,\*</sup> Xuerun Li,<sup>a,c</sup> Yusheng Shen<sup>a</sup> and Xiaodong Shen<sup>a\*</sup>

<sup>a</sup>State Key Laboratory of Materials-Oriented Chemical Engineering, College of Materials Science and Engineering, Nanjing Technology University, Nanjing 210009, People's Republic of China, <sup>b</sup>Donghai Advanced Silicon-Based Materials Institute, Nanjing Technology University, Donghai 222300, People's Republic of China, and <sup>c</sup>Laboratory of Construction Materials, Ecole Polytechnique Fédérale de Lausanne (EPFL), Lausanne CH-1015, Switzerland. \*Correspondence e-mail: mltang@njtech.edu.cn, xdshen@njtech.edu.cn

Received 31 August 2014

Accepted 9 April 2015

Edited by J. M. García-Ruiz, Instituto Andaluz de Ciencias de la Tierra, Granada, Spain

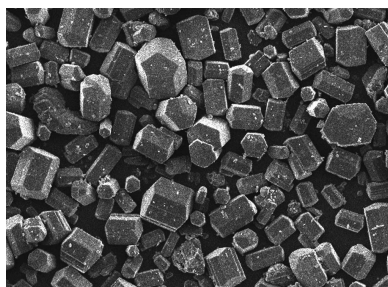
**Keywords:**  $\alpha$ -hemihydrate; flue gas desulfurization; gypsum; modeling; hydrothermal crystal growth; nonlinear optimization.

Modeling of the kinetics of the synthesis process for calcium sulfate  $\alpha$ -hemihydrate from gypsum formed by flue gas desulfurization (FGD) is important to produce high-performance products with minimal costs and production cycles under hydrothermal conditions. In this study, a model was established by horizontally translating the obtained crystal size distribution (CSD) to the CSD of the stable phase during the transformation process. A simple method was used to obtain the nucleation and growth rates. A nonlinear optimization algorithm method was employed to determine the kinetic parameters. The model can be successfully used to analyze the transformation kinetics of FGD gypsum to  $\alpha$ -hemihydrate in an isothermal batch crystallizer. The results showed that the transformation temperature and stirring speed exhibit a significant influence on the crystal growth and nucleation rates of  $\alpha$ -hemihydrate, thus altering the transformation time and CSD of the final products. The characteristics obtained by the proposed model can potentially be used in the production of  $\alpha$ -hemihydrate.

## 1. Introduction

Gypsum is one of the most popular calcium sulfate-based minerals. It can be found in buildings and statues from two thousand years ago and is currently quite widely used around the world as an important cementing material (Valimbe & Malhotra, 2002; Butalia *et al.*, 2001; Leiva *et al.*, 2010). Calcium sulfate presents as three distinct minerals: gypsum (the dihydrate,  $\text{CaSO}_4 \cdot 2\text{H}_2\text{O}$ ), hemihydrate (bassanite,  $\text{CaSO}_4 \cdot 0.5\text{H}_2\text{O}$ ) and anhydrite (anhydrous,  $\text{CaSO}_4$ ) (Freyer & Voigt, 2003). The transformation of these phases into each other, especially that of dihydrate to hemihydrate, is the basis for the application of calcium sulfate-based materials. The general application of calcium sulfate is the transformation of calcium sulfate dihydrate into hemihydrate by dehydration and the consequent crystallization of dihydrate.

Hemihydrate generally presents as  $\alpha$ - or  $\beta$ -hemihydrate according to the dehydration conditions (Charola *et al.*, 2007), and both can determine the performance of gypsum products. Although  $\beta$ -hemihydrate is produced extensively on an industrial scale,  $\alpha$ -hemihydrate also shows promising prospects owing to its high performance. Increasing attention has been given to  $\alpha$ -hemihydrate in the past two decades (Zurz *et al.*, 1991; Yu *et al.*, 2006; Guan *et al.*, 2009). Pioneering studies (Cheng *et al.*, 1995; Jiang & Luan, 2006; Duan *et al.*, 2008; Yu & Wang, 1996) indicated that an optimal shape and crystal size distribution (CSD) are necessary to achieve high-performance  $\alpha$ -hemihydrate crystals. Among all the current



© 2015 International Union of Crystallography

production methods, the hydrothermal process is the best choice for producing  $\alpha$ -hemihydrate crystals with precise particle properties, by which  $\text{CaSO}_4 \cdot 2\text{H}_2\text{O}$  is transformed into  $\alpha$ -hemihydrate in a solvent *via* crystallization under high temperature and pressure.

Cardew and Davey (Cardew & Davey, 1985; Davey *et al.*, 1986) discovered that the hydrothermal synthesis of  $\alpha$ -hemihydrate follows a two-step process. First,  $\text{CaSO}_4 \cdot 2\text{H}_2\text{O}$  dissolves in water, thereby elevating the concentration of calcium sulfate to the supersaturation point of  $\alpha$ -hemihydrate. Second,  $\alpha$ -hemihydrate crystals form and grow continuously until  $\text{CaSO}_4 \cdot 2\text{H}_2\text{O}$  is completely consumed. The CSD of  $\alpha$ -hemihydrate crystals is a result of competition between the nucleation and growth kinetics, similar to general crystallization in solution.

Two types of crystallizers are widely used to investigate crystallization kinetics. One is the mixed-suspension mixed-product removal crystallizer, and the other is the batch crystallizer. A batch crystallizer was used for the present work because the raw material [flue gas desulfurization (FGD) gypsum] was mixed with the product ( $\alpha$ -hemihydrate) during the course of the phase transformation.

Despite the simplicity of batch crystallization experiments, kinetics modeling requires complex calculations. Many studies have addressed both the numerical solution of a number balance equation (Qamar & Warnecke, 2008; Hu *et al.*, 2005a; Tadayon *et al.*, 2002; Li, 2003) and the kinetic parameter estimation (Nývlt & Karel, 1993; Hu *et al.*, 2005b; Liu *et al.*, 2004; Yokota *et al.*, 2000; Ouzazzane *et al.*, 2008) in the field of batch crystallization kinetics modeling. However, both solvent-mediated phase transformation and kinetic modeling have only rarely been addressed in the past. The underlying reasons are mainly the differences between the solvent-mediated phase transformation and solution crystallization, and the difficulty in establishing supersaturation. To achieve supersaturation of solution crystallization, a chemical reaction, a temperature change, solvent evaporation and variation of solvent composition have all been proposed (Myerson, 2002). Regarding the solvent-mediated phase transformation, supersaturation is obtained by continuous dissolution of the metastable phase, which is mixed with the stable phase. Thus, obtaining the CSD of the stable phase in the overall process is difficult for solvent-mediated phase transformation.

Moreover, high temperature and pressure make the endeavor more difficult for phase transformation under hydrothermal conditions. To date, even though the importance of understanding the kinetics of  $\alpha$ -hemihydrate formation is widely accepted from the point of view of industrial production and crystallizer design, no study has modeled the kinetics of  $\alpha$ -hemihydrate production and phase transformation under hydrothermal conditions.

A kinetic model of the  $\alpha$ -hemihydrate hydrothermal production process in an unseeded batch crystallizer was accomplished through the CSD horizontal translation method. In addition, the parameters of the kinetic empirical formulae have been estimated, which are believed to be of great value in the production of  $\alpha$ -hemihydrate.

## 2. Kinetic modeling

The following assumptions were made before performing the modeling, in order to simplify the calculations:

- (1) The crystallizer effectively mixes the materials, so all associated phenomena, such as crystal breakage, agglomeration and crystal growth rate dispersion, are negligible.
- (2) The growth rate is independent of crystal size, and the crystals only grow to a certain size.
- (3) All the crystals are of a similar shape.

### 2.1. Crystal size distribution derivations

Myerson (2002) noted that a comprehensive discussion of crystallization must include the factors that determine the size and size distribution, as well as their possible measurement and control. Although the CSD is required to model the phase transformation process, it is usually unavailable. Assuming that the growth rate is size independent, the entire distribution of stable-phase crystals is simply translated without changing the crystal number density. Thus, the CSDs of the stable phase at any time during the process can be obtained by translating the CSD of the final product. Fig. 1 shows two CSDs, one for the final product,  $n(L, t_f)$ , where  $L_0 \leq L \leq L_{\max}$ , and the other for the stable phase at time  $t$ ,  $n(L, t)$ . If the CSD of the final product can be obtained by moving along the abscissa to the left by a length  $L_g(t)$ , then  $n(L, t) = n[L + L_g(t), t_f]$ , where  $L_0 \leq L \leq L_{\max} - L_g(t)$ .

At this time, the volume of the stable phase  $V_s$  can be calculated by equation (1):

$$\begin{aligned}
 V_s &= \varphi_v \int_{L_0}^{L_{\max}} n(L, t) L^3 dL = \varphi_v \int_{L_0}^{L_{\max} - L_g(t)} n[L + L_g(t), t_f] L^3 dL \\
 &= \varphi_v \int_{L_0 + L_g(t)}^{L_{\max}} n(L, t_f) [L - L_g(t)]^3 dL, \quad (1)
 \end{aligned}$$

where  $\varphi_v$  is the volume shape factor of the stable phase. If  $V_s$  is known, then  $L_g(t)$  can be calculated. After that,  $n(L, t)$  can be derived, and the kinetics can also be calculated from  $n(L, t)$ .

To derive  $V_s$ , the volume proportion of the stable phase in the solid phase at time  $t$  should be known. Regarding the calcium sulfate phase transformation, the crystalline water

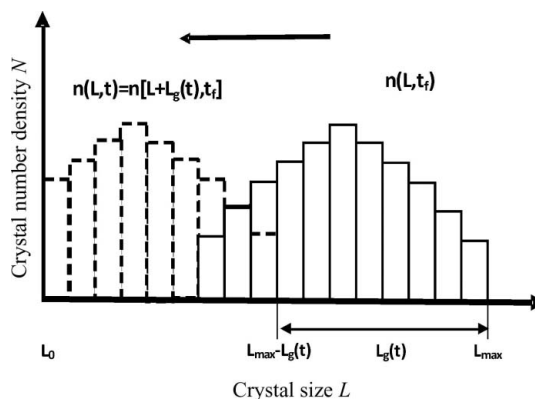


**Figure 1**  
The horizontal translation of the CSD of the final product to obtain the CSD of the stable phase.

content changes with time and becomes constant at the end of the transformation. The change in water content reflects the change in the amount of  $\alpha$ -hemihydrate because of the poor solubility of calcium sulfate and hence its negligible dissolution. These changes can be detected by dehydration of the samples.  $V_s$  can be finally determined.

In the batch crystallizer, the volume and specific surface area of the stable-phase crystals change continuously with time because of crystal growth and nucleation. The horizontal translation relation described above can only exist in the number CSD. Thus, the volume CSD of the final product must be converted to the number CSD.

## 2.2. Kinetic analysis

The population balance equation [equation (2)] is a popular model for the kinetics of a solution. The equation was first proposed by Hulbert & Katz (1964) and subsequently enhanced by Randolph & Larson (1988). This equation is also applicable to the calcium sulfate phase transformation under hydrothermal conditions, since it is also a crystallization process.

$$\frac{\partial n(L, t)}{\partial t} = G(t) \frac{\partial n(L, t)}{\partial L} \quad (0 < t < \infty, 0 < L < \infty), \quad (2)$$

with the initial condition

$$n(L, 0) = n_0(L), \quad (3)$$

and the boundary condition

$$n(0, t) = \frac{B(t)}{G(0, t)}. \quad (4)$$

The population balance equation is a partial differential equation in both time and size, and can be solved by numerical methods (Qamar & Warnecke, 2008; Hu *et al.*, 2004, 2005a; Tavaré & Garside, 1986; Mersmann *et al.*, 2002). These methods can solve the equation relatively easily, but they are not applicable to this system because the expression is more complicated than those obtained by direct measurement (the CSDs of the stable phase are translated). The calculation becomes extremely complex when using these methods.

Crystal growth is independent of crystal size in our model. The changes in crystal size with time are calculated as the growth rate. Among the final products, the largest crystal is formed at the beginning of the transformation. Its growth process is merely the reverse of the CSD translation process shown in Fig. 1. Thus, the crystal growth rate  $G(t)$  can be calculated by equation (5):

$$G(t) = \frac{-dL_g(t)}{dt}, \quad (5)$$

where  $L_g(t)$  has already been defined in this study.

The nucleation rate can be calculated by the boundary condition  $B(t)$  of the population balance equation [equation (4)].

$$B(t) = n(0, t) G(0, t). \quad (6)$$

Based on the assumption of this model, the crystals are formed at a certain size,  $L_0$ :

$$n(0, t) = n(L_0, t) = n[L_0 + L_g(t), t]. \quad (7)$$

If crystal growth is independent of size,

$$G(0, t) = G(t). \quad (8)$$

Thus,

$$B(t) = n[L_0 + L_g(t), t] G(t). \quad (9)$$

## 2.3. Kinetic parameter estimation

Once the kinetics of nucleation and growth are known, the next step is to correlate the kinetics with the operation conditions. The crystal growth and nucleation rates depend on the degree of supersaturation, the temperature, the concentration of impurities and the hydrodynamic conditions in the crystallizer. As a result, the crystal growth and nucleation rates can be modeled by an empirical power law, expressed in equations (10) and (11):

$$B(t) = K_b \sigma^b M_T^e N^f, \quad (10)$$

$$G(t) = K_g \sigma^g N^p. \quad (11)$$

Here,  $K_b$  is the nucleation rate coefficient, which may depend on the temperature, the hydrodynamics, the presence of impurities and the crystal properties.  $\sigma [= (C - C^*)/C^*]$  is the relative supersaturation, where  $C$  is the solution concentration at time  $t$  and  $C^*$  is the equilibrium saturation.  $M_T$ , the magma density ( $\text{g cm}^{-3}$ ), accounts for secondary nucleation effects and can be calculated by the content of the stable phase in the solid phase.  $N$  is the stirring speed ( $\text{r min}^{-1}$ ).  $K_g$  is the growth rate coefficient, which depends on the temperature, the hydrodynamics and the presence of impurities in the solution.

Equations (10) and (11) are nonlinear equations, the parameters of which can only be estimated by certain numerical methods. Herein, a nonlinear optimization algorithm was applied to solve these equations. The objective function that accounts for the differences between the experimental and model prediction values of the kinetics behavior is given by equation (12):

$$\min_{\theta} \varphi_v(\theta) = \sum_{i=1}^{n_e} \sum_{j=1}^{n_s} [y_{ij,m} - y_{ij}(\theta)]^2, \quad (12)$$

where  $\theta$  is the kinetic parameter vector,  $y_{ij,m}$  and  $y_{ij}(\theta)$  are the experimental and simulated values, respectively, of the  $j$ th size band in the  $i$ th experimental run, and  $n_e$  and  $n_s$  are the number of experiments and the number of size bands in the CSD of the final product, respectively. Two optimization steps were employed to obtain the related parameters. First,  $y_{ij}$  represented the crystallization rate, solving the parameters in equation (11). With these obtained parameters, the second optimization was done by combining  $B$  and  $G$  as equation (13) to represent the volume of  $\text{CaSO}_4 \cdot 0.5\text{H}_2\text{O}$ :

$$y_{ij}(\theta) = \varphi_v N_j r_j^3 = \varphi_v \left(\frac{B}{G}\right) r_j^3 = \frac{\varphi_v K_b \sigma^b M_T^e N_j^f r_j^3}{(K_g \sigma^g N_j^p)}, \quad (13)$$

where  $N_j$  and  $r_j$  are the crystal number and size of the  $j$ th size band, respectively, and  $N_i$  is the stirring speed of the  $i$ th experiment.

When the difference between the measured and simulated values reaches a minimum value, the parameters of equations

(10) and (11) can be obtained. The process for the solution is shown in Fig. 2. Here we do the optimization twice to obtain all the parameters. In the first optimization,  $y_{ij,m}$  and  $y_{ij}(\theta)$  represent the crystallization rate obtained experimentally (derived by equations) and that obtained by modeling (calculated using the nucleation equation), respectively, and from here we can obtain  $K_g$ ,  $g$  and  $p$ . In the second optimization,  $y_{ij,m}$  represents the crystal volume of  $\alpha$ -hemihydrate at every particle range and  $y_{ij}(\theta)$  is the crystal volume at each particle range obtained by the nucleation and growth equation, and then the remaining parameters can be obtained as coupled relationships, such as  $K_b N_f = \text{constant}$  for equation (10) and  $K_g N_p = \text{constant}$  for equation (11). More than two sets of experimental data could solve these coupled equations, which means  $N_e$  must be at least 2.

In equation (12), seven parameters must be determined. If one experiment were conducted, only  $b$ ,  $e$  and  $g$  could be obtained. To evaluate all of these parameters,  $n_e$  should not be less than 2, which means that there should be at least two sets of experiments. If the parameters of the stirring speed are not involved in equations (10) and (11), one experiment is sufficient to obtain all the parameters. Moreover, the volume of the final product is included in the parameter estimation, and the estimated parameters are appropriate for the volume CSD simulation of the product. As a number of CSD simulations are required, the parameter estimation must accordingly be based on the number of CSDs. The weight coefficient should also be considered in the optimization process because of the significant differences in crystal number between experiments.

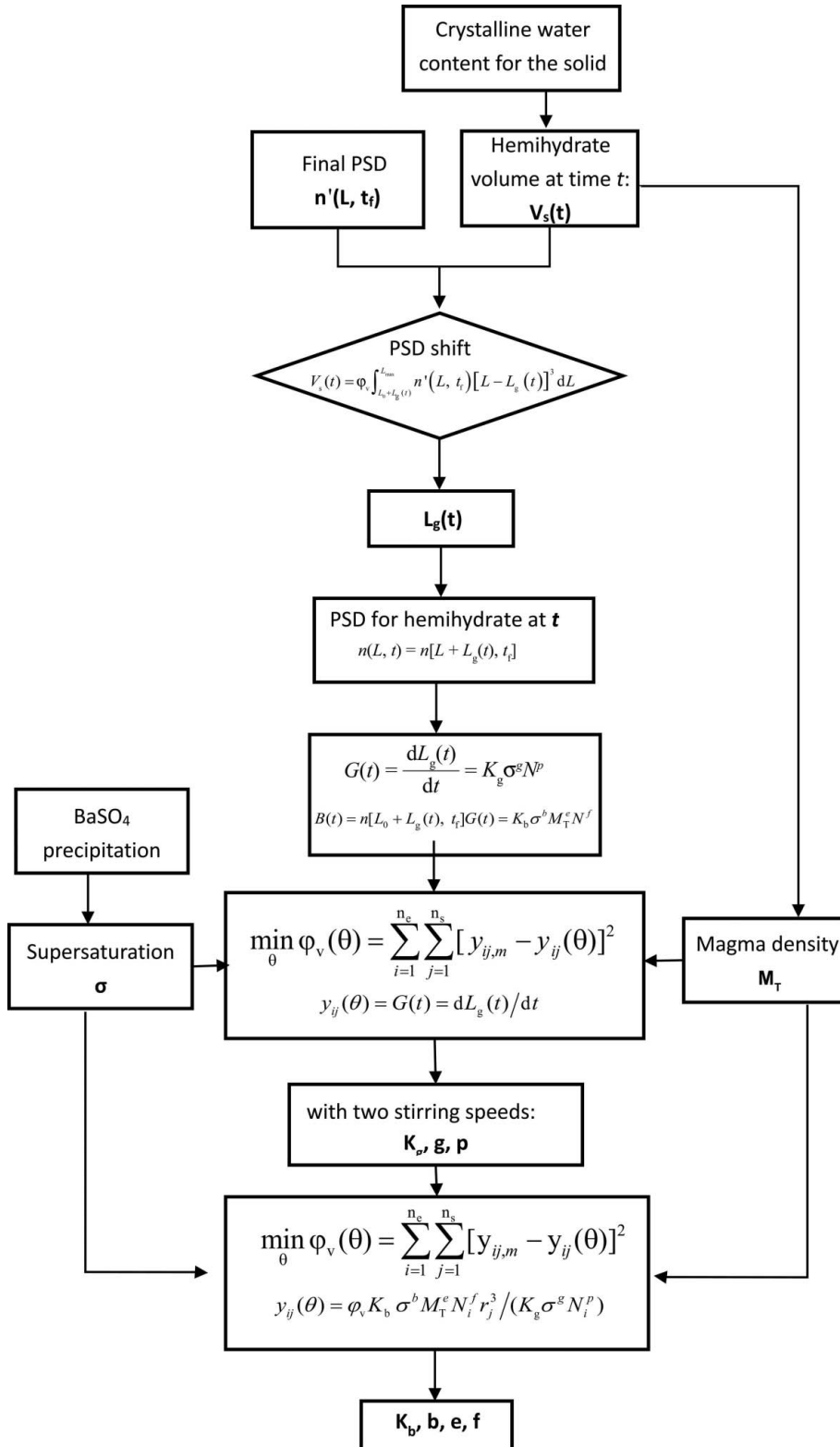


Figure 2 The solution process for the equations.

### 3. Experimental

#### 3.1. Materials

FGD gypsum with 94.0%  $\text{CaSO}_4 \cdot 2\text{H}_2\text{O}$  content was obtained from a thermal power plant in Nanjing, China. The morphology and CSD of the FGD gypsum are shown in Fig. 3. The majority of the raw crystals of the FGD gypsum are sheet-like elliptical particles with a rough surface and a size of

approximately 30  $\mu\text{m}$ . A small number of crystals smaller than 10  $\mu\text{m}$  can be found in the particle size distribution curves (see Fig. 3*b*). The solution used to seed the crystallization was composed of 0.10% succinic acid and 99.90% distilled water.

### 3.2. Apparatus

The experimental apparatus was composed of an 8 l jacketed batch crystallizer equipped with a propeller-type stirrer with variable stirring speeds, ranging from 150 to 1000  $\text{r min}^{-1}$ . The crystallizer was heated in an oil bath with a temperature error of  $\pm 0.5$  K.

### 3.3. Experimental procedure

The slurry, a mixture of 5.0 kg of solution and 3.33 kg of FGD gypsum, was placed into the crystallizer and then heated in an oil bath. As soon as the slurry reached the target temperature, the transformation was initiated (time  $t$  was considered to be zero at this point). First, the initial transformation temperature was determined as 400.6 K. For a specific initial temperature maintained for 3 h, we checked for the existence of crystals to decide whether the initial temperature should be raised. If there were no crystals, the temperature was then increased by 1 K. For the experiment carried out at 400.6 K,  $t = 0$  was used as the initial point of crystallization, which was reasonable.

To simplify the calculations, any nucleation or growth before the initial time was ignored. A 5–10 ml aliquot of solution and a small amount of the slurry sample were pumped out every 5–20 min during crystallization. The slurry was isolated by vacuum micro-filtration and immediately washed with hot water and ethanol. Next, the solid samples were dried at  $318 \pm 5$  K. The combined water content of the dried samples was measured by dehydration of the sample in an oven at 503 K for 45 min, according to Chinese standard

GBT 17669.2-1999. The CSD of the final product was measured using a Malvern MS2000 laser diffraction granulometer. Supersaturation of the solution samples was measured chemically by detecting  $\text{SO}_3$  content using gravimetric sulfate determination by  $\text{BaSO}_4$  precipitation. An aqueous solution of barium chloride was added in excess to precipitate barium sulfate, and the precipitate was digested in the hot solution. The precipitate was filtered through a quantitative filter paper, which was then ignited and completely washed. From the weight of the sample and the weight of the precipitate, the percentage of sulfate in the sample was calculated. Foreign anions and cations could influence the precision of the results. Good operation can decrease the error in the testing. In our

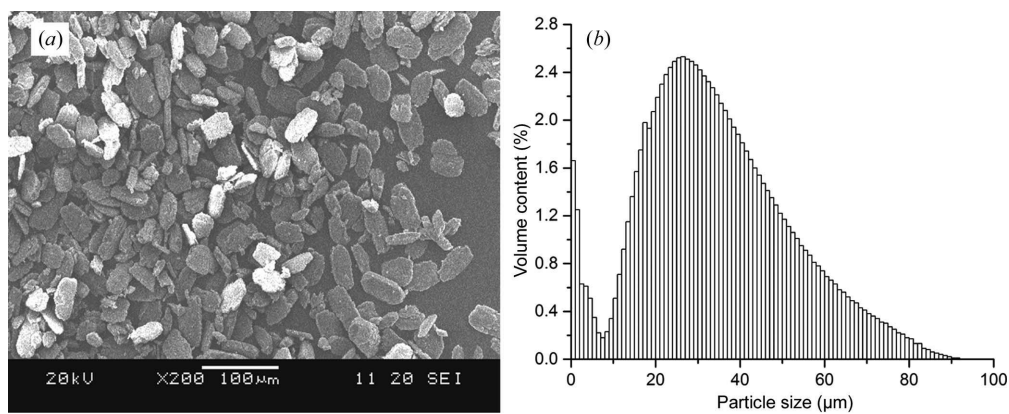


**Figure 3**  
(a) The morphology of the FGD gypsum used in this study and (b) its CSD.

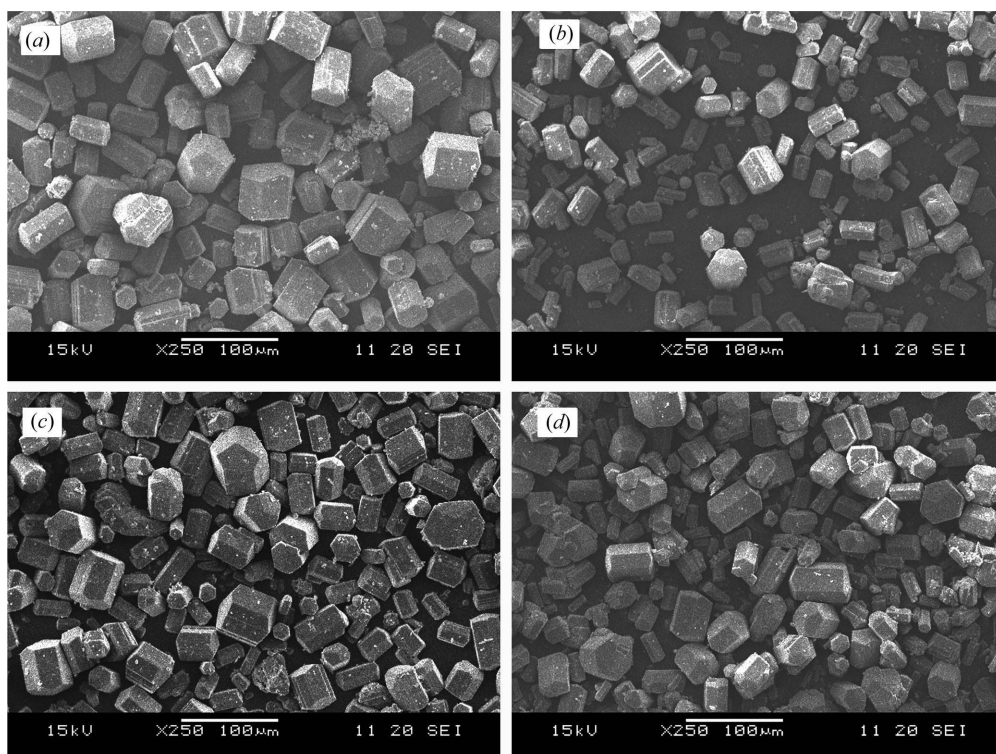


**Figure 4**  
SEM photographs of the final products. (a) Run 1, (b) Run 2, (c) Run 3 and (d) Run 4.

**Table 1**  
Operating conditions for the experiments.

Runs	Transformation temperature (K)	Stirring speed (r min <sup>-1</sup> )	Transformation time (min)
Run 1	400.6	100	250
Run 2	400.6	150	225
Run 3	402.6	100	175
Run 4	402.6	150	135

sample, the FGD gypsum contains a relatively low proportion of foreign ions. An ideal precision (relative error less than 0.1%) for chemical testing could be achieved.

In total, four runs of the experiments were performed for this study. The operating conditions and transformation times are listed in Table 1.

## 4. Results and discussion

### 4.1. Morphology

The volume CSD data obtained by the granulometer must be converted to the number CSD, as required by the model. Special care should be taken in the CSD conversion process, as even a small volume of small crystals can be enlarged into a significant part of the number distribution. If this small volume arises from errors in the measurement it can interfere with the actual distribution, thereby resulting in a significant influence on the kinetic analysis. When the solid is isolated from the slurry samples, tiny crystals can be washed away from the holes in the filter paper (pore size range 1–3 μm). In addition, it is difficult to separate the small crystals completely from the filter paper because they adhere to it. Fortunately, this volume of small crystals is too small to disturb the kinetic analysis, given careful operation. Specifically, crystals smaller than 10 μm are excluded in all calculation processes, considering the pore size of the filter paper and the scanning electron microscopy (SEM) pictures of the final products (Fig. 4).

From Fig. 4, all the final products are found to have a similar morphology, and little agglomeration has occurred among the crystals. The crystals have the appearance of uniformly rounded hexagonal cylinders with well crystallized surfaces. The growth of the crystals is mainly along the radial direction for both small and large crystals. The similarity of the morphology of the crystals guarantees the validity of the calculations that are the basis for this method.

The assumption made above is reasonable and it is supported on solid grounds. Taking the variation in temperature into consideration, a 2 K increment in the crystallization temperature exhibited little influence on the morphology of the resulting crystals. Differences in the CSD were also observed from the SEM images; a more precise measurement of the CSD of the crystal is presented in the following section through the use of the granulometer.

### 4.2. Parameter estimation

Based on the measurement of the calcium sulfate concentration and the crystal water content (gravimetric sulfate

**Table 2**  
Estimated kinetic parameters for two transformation temperatures.

Kinetic parameter	Estimated value	
	400.6 K	402.6 K
$K_b$	$7.167 \times 10^{-2}$	2.864
$b$	2.431	1.966
$e$	0.733	0.739
$f$	4.047	3.734
$K_g$	0.940	$6.701 \times 10^{-2}$
$g$	1.044	1.079
$p$	0.168	0.763

determination by BaSO<sub>4</sub> precipitation, as described above), the calculated relative supersaturation and the hemihydrate magma density are shown in Fig. 5.

The relative supersaturation characteristics for the specific runs were obtained *via* the calcium sulfate concentration according to the chemical method, as shown in Fig. 5(a). Specifically, a few data points at the very start of the reactions for Runs 3 and 4 seem to be abnormal, which could be attributed to operation error.

As shown in Fig. 5(b), the hemihydrate magma density is obtained from the crystal water content data, and shows

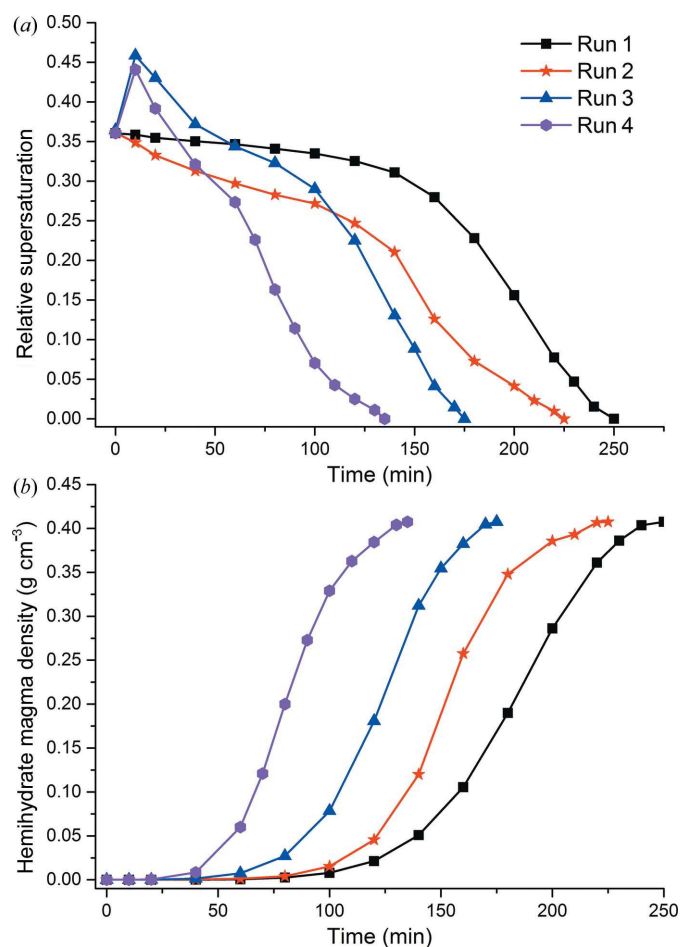


**Figure 5**  
(a) The evolution of the relative supersaturation of  $\alpha$ -hemihydrate,  $\alpha$ -CaSO<sub>4</sub>·0.5H<sub>2</sub>O. (b) The evolution of the magma density of  $\alpha$ -CaSO<sub>4</sub>·0.5H<sub>2</sub>O.

typical sigmoid curves that usually imply the underlying nucleation and growth kinetics.

Using the least-squares method, the kinetics models [equation (13)] of transformation at 400.6 and 402.6 K were solved. To estimate the kinetic parameters, two experimental runs were performed for parameter estimation for one transformation temperature. Run 1 and Run 2 were performed at 400.6 K, and Run 3 and Run 4 were performed at 402.6 K. MATLAB software (MathWorks, Natick, Massachusetts, USA) was used to simplify the calculation processes. The parameters estimated are presented in Table 2.

From the estimated parameters, the relative supersaturation ( $\sigma$ ) exerts a significant influence on both the nucleation and growth rates for  $\alpha$ -hemihydrate crystals: the exponent  $g$  for supersaturation is close to 1 [see equation (13)]. The stirring speed ( $N$ ), controlling the parameters  $f$  and  $p$ , exhibits the most important influence on the nucleation rate, and the exponents for both temperatures are all as high as approximately 4.0. This result is most likely because the temperature at which the phase transformation occurs spontaneously in this system is approximately 399.6 K and the transformation temperatures used in this study (400.6 K and 402.6 K) are only slightly higher. The  $\alpha$ -hemihydrate crystals are mostly produced by secondary nucleation; for most industrial crystallization, secondary nucleation, originating from contact

nucleation caused by rubbing and impact, is the most usual nucleation process (Myerson, 2002), and the contact energy generated by the agitation of the propeller is an important factor for producing secondary nuclei.

The stirring speed also has an influence on the growth rate, and this influence is much more obvious at higher temperatures. Agitation can (or may) increase the dissolution of  $\text{CaSO}_4 \cdot 2\text{H}_2\text{O}$  and reduce the dependence of the transformation rate on the dissolution rate of  $\text{CaSO}_4 \cdot 2\text{H}_2\text{O}$ . At higher temperatures, the growth of the crystals is diffusion controlled (Mersmann, 2001), and agitation can promote solute mass transfer and change the growing speed.

#### 4.3. CSD simulation

The measured and simulated volume CSDs of all four runs are shown in Fig. 6. The simulated CSDs are obtained through equations (10) and (11). From Fig. 6, the simulated CSDs of the four runs provide good fits to the measured CSDs for small crystal sizes. The errors between the model and the experimental results increase with increasing crystal size (see Figs. 6 and 7). Potential cracking of the large crystals may be responsible for the mismatch. In assumption (1), it was assumed that the growth of the crystal has no impact on the crystal size. However, with the growth of the crystals in

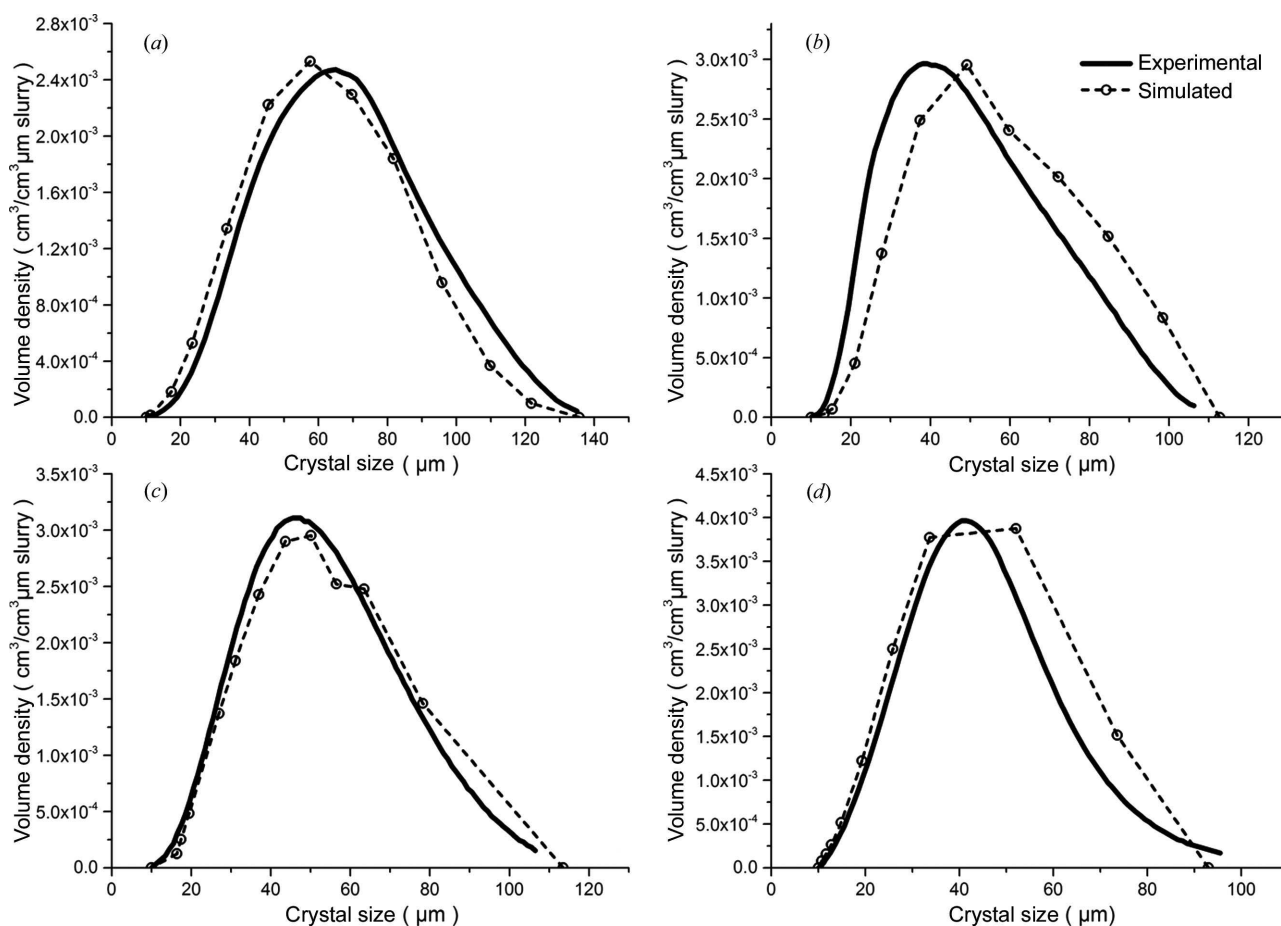


**Figure 6**  
The experimental and simulated volume CSDs of the final products. (a) Run 1, (b) Run 2, (c) Run 3 and (d) Run 4.

practice there would be more defects and a bigger momentum for the larger crystals, which would be more easily crushed in subsequent contact with the inner surface of the reactor and the rotating stirrer. This would cause the measured CSD for the crystals to be shifted to small sizes. Furthermore, an increased stirring speed yielded more crushed crystals, so the mismatch was bigger.

Assumption (2) aimed to simplify the calculation and make this type of model applicable to the crystallization process. The mismatch between the obtained model and the practical process demonstrates the drawback of this sort of simplification of the process. This also shows that the model can be improved by correcting the equation with a consideration of defects and crystal size. Here, we have provided a simple and practical model to deal with the crystallization process and a possible approach to improve the forthcoming application of the model.

Nevertheless, the kinetic equations can simulate the process well on an industrial scale, and the modeling method can be used to analyze the kinetics of solvent-mediated phase transformation, such as the preparation of  $\alpha$ -hemihydrate from FGD gypsum under hydrothermal conditions.

The kinetics of the process can be understood using all the process data (such as supersaturation and crystal magma density), the evaluated parameters and the CSDs of the

products. The CSDs of the final products and the transformation rates result from competition between crystal nucleation and growth. A thorough understanding of the crystallization mechanism can benefit the industrial production of  $\alpha$ -hemihydrate with optimized CSDs. The effect of the temperature, the stirring speed and the characteristics of the metastable phase on the crystallization processes can be properly controlled. Only when the production process is well controlled can the quality of the products be optimized. The method proposed here to solve the model can be used widely, and more precise results will be obtained with up-to-date techniques for the more stable and precise measurement of solution supersaturation and magma density. Correcting the equation by taking the crushing of the large crystals into account would further improve the accuracy of the model.

The results of the modeling are also applicable to other types of calcium sulfate (hemihydrate, anhydrite). The model can also be used for seeded solvent-mediated phase transformations, providing that size-independent growth is strictly satisfied.

### 5. Conclusions

The proposed model has interpreted the kinetics of calcium sulfate transformation under hydrothermal conditions by

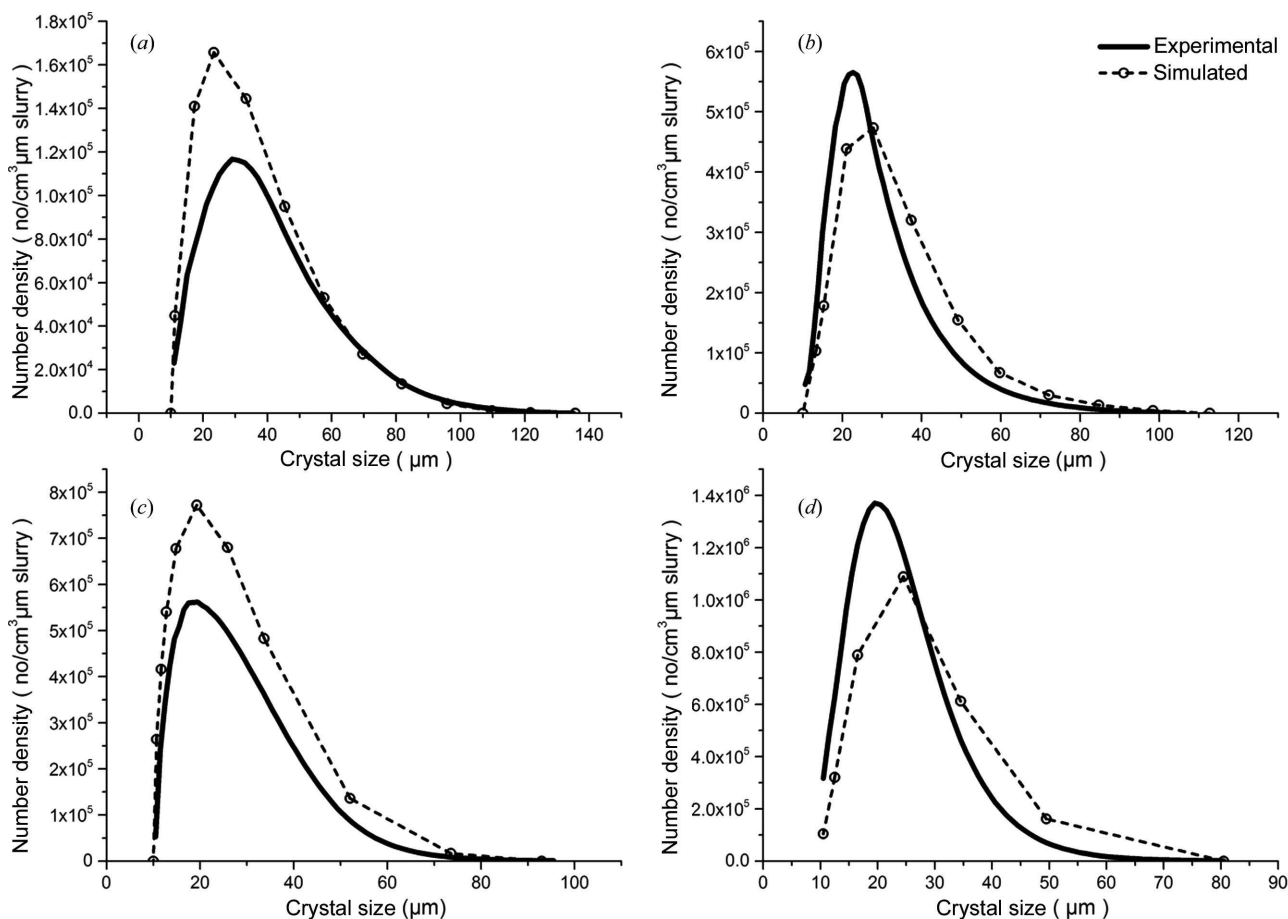


Figure 7 Plots of the experimental and simulated number densities versus crystal size for the final products. (a) Run 1, (b) Run 2, (c) Run 3 and (d) Run 4.

moving the CSD of the final product horizontally. The CSDs of the  $\alpha$ -hemihydrate product simulated by the kinetic parameters fitted the experimental CSDs reasonably well; the resulting kinetic equations could precisely simulate the transformation process.

Kinetics modeling benefits the production of  $\alpha$ -hemihydrate from FGD gypsum. The stirring speed and temperature have a remarkable influence on  $\alpha$ -hemihydrate formation. The most important factor governing the reaction is temperature, which can change the nucleation and growth rates, thus resulting in a tremendous change in the CSD of the final product. Secondary nucleation still governs the formation of crystals in this system, even though the primary nucleation rate initiates the transformation.

### Acknowledgements

The authors are grateful for funding of this project by the Priority Academic Program Development of Jiangsu Higher Education Institutions (PAPD), and acknowledge the Program for Changjiang Scholars and Innovative Research Team in University (PCSIRT, grant No. IRT1146), the National Building Materials Industry Technological Innovation Projects (grant No. 2013-M4-3), and the National Key Technology Research and Development Program of the Ministry of Science and Technology of China (grant No. 2014BAL03B04).

### References

- Butalia, T. S., Wolfe, W. E. & Lee, J. W. (2001). *Fuel*, **80**, 845–850.
- Cardew, P. T. & Davey, R. J. (1985). *Proc. R. Soc. London Ser. A*, **398**, 415–428.
- Charola, A. E., Puhlinger, J. & Steiger, M. (2007). *Environ. Geol.* **52**, 207–220.
- Chen, C., Chen, B., Zhang, X. & Li, Q. (1995). *J. Fuzhou Univ. Nat. Sci. Ed.* **23**, 100–103.
- Davey, R. J., Cardew, P. T., McEwan, D. & Sadler, D. E. (1986). *J. Cryst. Growth*, **79**, 648–653.
- Duan, Z., Qin, H., Li, G., Tang, X. & Wen, Z. (2008). *New Building Mater.* **2008(8)**, 1–4.
- Freyer, D. & Voigt, W. (2003). *Monatsh. Chem.* **134**, 693–719.
- Guan, B., Yang, L., Wu, Z., Shen, Z., Ma, X. & Ye, Q. (2009). *Fuel*, **88**, 1286–1293.
- Hu, Q., Rohani, S. & Jutan, A. (2005a). *AIChE J.* **51**, 3000–3006.
- Hu, Q., Rohani, S. & Jutan, A. (2005b). *Comput. Chem. Eng.* **29**, 911–918.
- Hu, Q., Rohani, S., Wang, D. X. & Jutan, A. (2004). *AIChE J.* **50**, 1786–1794.
- Hulburt, H. & Katz, S. (1964). *Chem. Eng. Sci.* **19**, 555–574.
- Jiang, H. & Luan, C. (2006). *J. Wuhan Univ. Technol.* **26**, 684–686.
- Leiva, C., García Arenas, C., Vilches, L. F., Vale, J., Gimenez, A., Ballesteros, J. C. & Fernández-Pereira, C. (2010). *Waste Manage.* **30**, 1123–1129.
- Li, S.-P. (2003). *Shanxi Chem. Ind.* **2003(3)**, 34–52.
- Liu, Y., Wang, J. K. & Wei, H. Y. (2004). *J. Cryst. Growth*. **271**, 238–244.
- Mersmann, A. (2001). *Crystallization Technology Handbook*. Boca Raton: CRC Press.
- Mersmann, A., Braun, B. & Loffelmann, M. (2002). *Chem. Eng. Sci.* **57**, 4267–4275.
- Myerson, A. (2002). *Handbook of Industrial Crystallization*. Oxford: Butterworth–Heinemann.
- Nývlt, J. & Karel, M. (1993). *Collect. Czech. Chem. Commun.* **58**, 1839–1847.
- Ouiazane, S., Messnaoui, B., Abderafi, S., Wouters, J. & Bounahmidi, T. (2008). *J. Cryst. Growth*, **310**, 798–803.
- Qamar, S. & Warnecke, G. (2008). *J. Comput. Appl. Math.* **222**, 715–731.
- Randolph, A. D. & Larson, M. A. (1988). *Theory of Particulate Processes*. New York: Academic Press.
- Tadayon, A., Rohani, S. & Bennett, M. K. (2002). *Ind. Eng. Chem. Res.* **41**, 6181–6193.
- Tavare, N. S. & Garside, J. (1986). *Chem. Eng. Res. Des.* **64**, 109–118.
- Valimbe, P. S. & Malhotra, V. M. (2002). *Fuel*, **81**, 1297–1304.
- Yokota, M., Sato, A. & Kubota, N. (2000). *Chem. Eng. Sci.* **55**, 717–722.
- Yu, D., Yang, X., Yang, S. & Zhang, L. (2006). *J. Wuhan Univ. Technol.* **28**, 27–29.
- Yu, W. & Wang, Z. (1996). *J. Wuhan Univ. Technol.* **18**, 1–4.
- Zurz, A., Odler, I., Thiemann, F. & Berghofer, K. (1991). *J. Am. Ceram. Soc.* **74**, 1117–1124.